LASER INTERFEROMETER GRAVITATIONAL WAVE OBSERVATORY
- LIGO -
CALIFORNIA INSTITUTE OF TECHNOLOGY
MASSACHUSETTS INSTITUTE OF TECHNOLOGY

| **Technical Note** | **LIGO-T1800359-v2** | April 4, 2018 |
|---|---|---|

# Pcal Gold Standard and Working Standard Configuration Change Proposal

Y. Lecoeuche, M. Szczepańczyk, R. Savage, S. Karki, T. Sadecki

**California Institute of Technology**
**LIGO Project, MS 18-34**
**Pasadena, CA 91125**
Phone (626) 395-2129
Fax (626) 304-9834
E-mail: info@ligo.caltech.edu

**Massachusetts Institute of Technology**
**LIGO Project, Room NW22-295**
**Cambridge, MA 02139**
Phone (617) 253-4824
Fax (617) 253-7014
E-mail: info@ligo.mit.edu

**LIGO Hanford Observatory**
**Route 10, Mile Marker 2**
**Richland, WA 99352**
Phone (509) 372-8106
Fax (509) 372-8137
E-mail: info@ligo.caltech.edu

**LIGO Livingston Observatory**
**19100 LIGO Lane**
**Livingston, LA 70754**
Phone (225) 686-3100
Fax (225) 686-7189
E-mail: info@ligo.caltech.edu

http://www.ligo.caltech.edu/

# 1 Introduction

This document describes the rationale behind the proposed configuration change for the Pcal Gold Standard and Working Standards. Part one reviews the current Working Standard/Gold standard setup, as well as the calculations that go into power sensor calibrations. Part two evidences the need for a reconfiguration of the Pcal Standards. Part three details measurements that have been taken to determine the source of the error for which the configuration change becomes necessary. Part four describes the factors taken into account in changing the standard. Part five presents the final configuration.

Calibration data is obtained in a lab setting as described in the PCal calibration procedure (T1400442).

Other documents drawn upon in this summary include:

- **LIGO-T1500036-v1** Index of Photon Calibrator Gold Standard and Checking Standard NIST calibrations
- **LIGO-T1500054-v75** Photon Calibrator Power Calibration Standard Trends
- **LIGO-T1400442-v3** Photon Calibrator Procedure for Measuring Response Ratios of Power Calibration Standards
- **LIGO-T070210-v6** Power Calibration Standard System Descriptions (Photon Calibrator Power Calibration)
- **LIGO-T1800207-v2** Historical Overview of Pcal Laser Power Calibration Standards

## 1.1 Summary

In summary, the main error source we wish to remove is a result of occluding apertures between the two detector spacers. We also find laser speckle and radial dependence to be significant potential sources of error, and we try to reduce the contributions from these sources as much as possible. The ideal configuration we choose for Working Standard and Gold Standard has zero spacers, a single piece for the photodetector housing/adapter, improved photodetector mounting on the integrating sphere, and a circuitboard with a built-in transimpedance amplifier.

## 1.2 Calibration factor

Laser power sensor are transducers converting incoming laser power $P$ on a photodiode to the voltage $V$:

$$V = \rho P, \tag{1}$$

where $\rho$ is a calibration factor with unit of $V/W$. The uncertainty of $\rho$ is one of the factors limiting calibration of the strain in GW data.

**Notation** Calibration factor:

$$\rho = \rho_0 \pm \delta\rho, \tag{2}$$

where $\rho_0$ is the value of the calibration factor and $\delta\rho$ is the uncertainty of the calibration factor.

Normalized calibration factor. The values of the calibration factors were changing over the years due to the modifications of the design, replacing the photodiode etc. In order to find out the stability of calibration factor over the years and make comparison we define the normalized calibration factor:

$$\rho_N = (\rho/\rho_{\text{mean}} - 1) \times 100\%, \tag{3}$$

where $\rho_{\text{mean}}$ is a mean of calibration factor values.

Uncertainty of the calibration factor $\delta\rho$ we define as a standard deviation:

$$\delta\rho = \sqrt{\frac{1}{N-1}\sum_{i=1}^{N}(\rho_i - \rho_{\text{mean}})^2}. \tag{4}$$

**Current design** Current GW/WS design is shown in Figure 1. The the current setup consists of:

- Integrating sphere - lined inside with a spectralon coating that scatters laser light to remove photodiode dependence on the incident angle of the laser. Laser enters through a 1/2" aperture and is collected through a 1/4" aperture. Sphere has a 4" diameter.
- Spacer 1 - Cylindrical adapter that attaches to the exit aperture on the integrating sphere. Implemented to reduce radial dependence of the photodetector mounting. 4/5" length, with a 1/32" aperture in the center of the spacer.
- Spacer 2 - Identical to Spacer 1, included to further reduce radial dependence of system.
- Photodiode and mounting - Photodiode and circuitboard housed in a square chassis that mounts to Spacer 2 and connects circuitboard to a BNC cable.

**Calibration Procedure** The Gold Standard, once calibrated by NIST in V/W, is used to calibrate a Working Standard, which is then used to calibrate the end station power sensors. This degree of separation exists to minimize potential strain and loss of calibration for the Gold Standard. For a laser entering the power sensor, the measured output is dependent on fluctuations in the laser power:

$$V_{GS} = P(t_1) * \rho_{GS} \qquad V_{WS} = P(t_2) * \rho_{WS} \tag{5}$$

In order to remove this, the Gold Standard and Working Standard outputs are measured simultaneously by directing the laser through a beam splitter and into both spheres. This

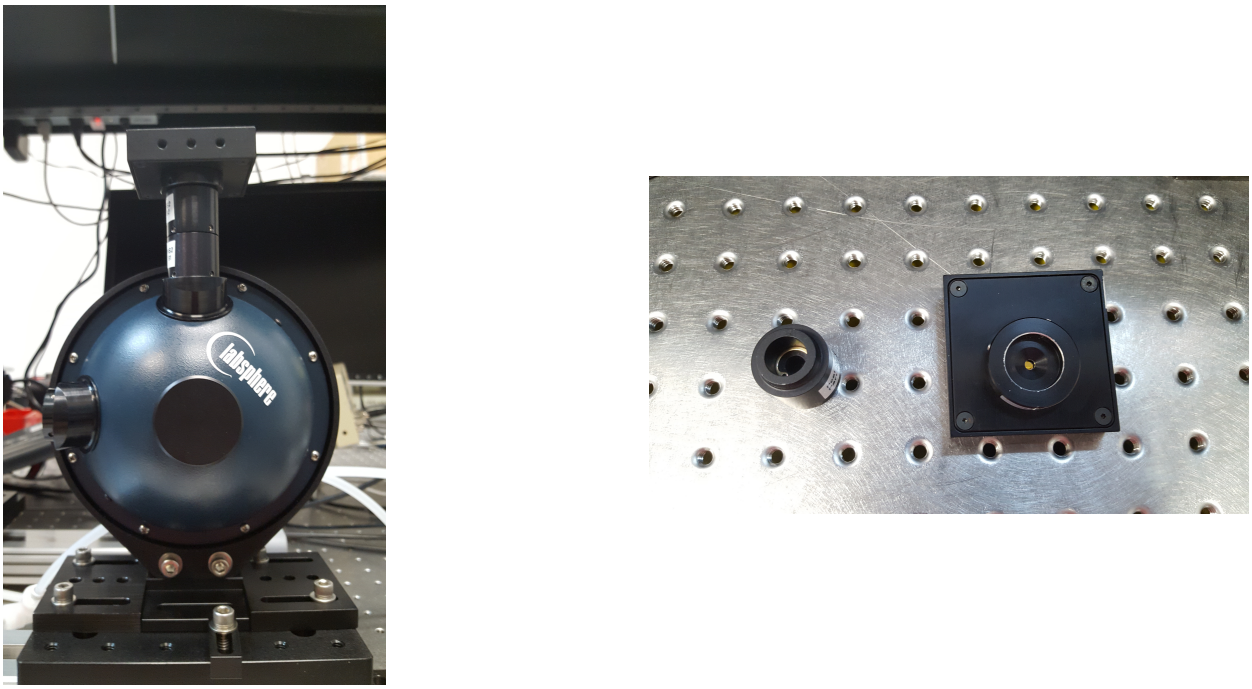


Figure 1: Power sensor design. Left: Integrating sphere attached at top to two spacers and photodetector. Mounted to a base at the bottom. Right: Detached spacer and photodetector.

makes P(t) the same for both measurements, but introduces factors for the transmission and reflection coefficients of the beam splitter:

$$V_{GS}(\text{at reflection}) = \alpha_R * P(t) * \rho_{GS} \qquad V_{WS}(\text{at transmission}) = \alpha_T * P(t) * \rho_{WS} \quad (6)$$

This dependence is removed by taking measurements for the Gold Standard and Working Standards at reflection and transmission. With this data we can calculate the calibration factor between the Standards:

$$\sqrt{\frac{V_{WS}(\text{refl}) * V_{WS}(\text{tran})}{V_{GS}(\text{refl}) * V_{GS}(\text{tran})}} = \sqrt{\frac{\alpha_R P(t_1)\rho_{WS}\alpha_T P(t_2)\rho_{WS}}{\alpha_T P(t_2)\rho_{GS}\alpha_R P(t_1)\rho_{GS}}} = \boxed{\frac{\rho_{WS}}{\rho_{GS}}} \quad (7)$$

The power sensor measurements also experience a phenomenon called laser speckle, wherein the scattered laser light shifts in and out of coherence, forming a moving speckle pattern on the photodiode. This effect is reduced by integrating laser measurements for ten minutes and then taking the average.

## 2 Summary of Working Standard History and WSH/GS Calibration Factor Offset

The calibration of the Pcal Working Standards to the Gold Standard has improved consistently since its start in 2008. The full set of calibration measurements made with the

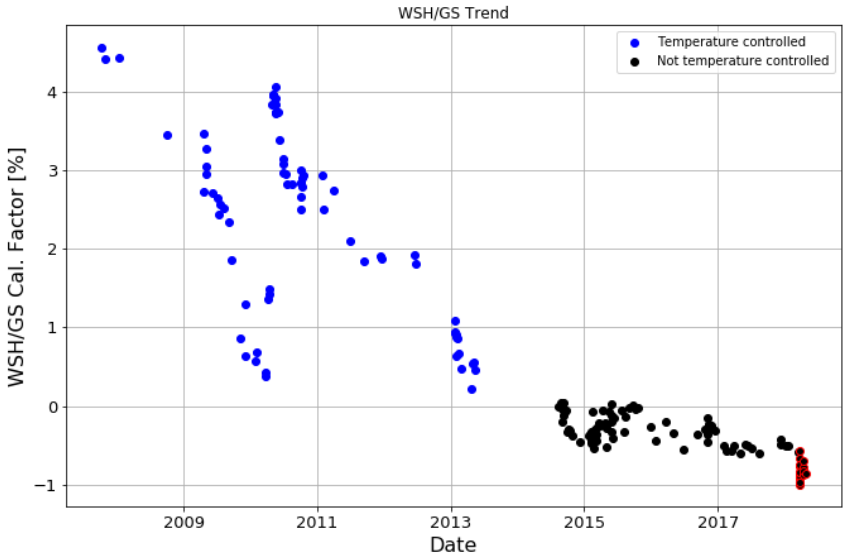


Figure 2: WSH/GS calibration factor measurements over the past 10 years. The previous temperature controlled configuration is shown in blue, the non-temperature controlled in black. Outlined in red are the offset values that prompted investigation.

Hanford Working Standard can be seen in Figure 2. This improvement stems from a range of changes made to the calibration system configuration, such as switching from a TEC-cooled InGaAs photodetector to a standard InGaAs photodetector and standardizing the calibration measurement technique. The standard deviation of data points goes from a normalized standard deviation of 1.176% in the early stages to 0.129% for recent measurements (excluding the offset values outlined in red). WS/GS calibration was, in its current state, thought to contribute 0.03% to the receiver module uncertainty until recent measurements proved otherwise.

Since late 2016, calibration measurements for LHO have been taken with Working Standard WS3, denoted later as WSH (Figure 3). The end set of WSH measurements shows a set of twelve measurements with an average 0.8% offset from previous measurements (shown outlined in red). The cause of the shift was unknown, as no significant changes to the Working Standard were recorded between the offset measurements and the measurement immediately preceding them. This offset is the reason that the power sensor configuration change was put forward.

## 2.1 Determining WSH as Error Source

After the offset was discovered, a set of experiments was conducted to determine the part of the calibration setup in error, as well as the source of said error. Concerned that the Gold Standard was in error, WSL/GS measurements were taken initially to attempt to rule it out (outlined in red in the left plot of Figure 4). The values obtained had no large offset and a similar spread to previous WSL/GS values.

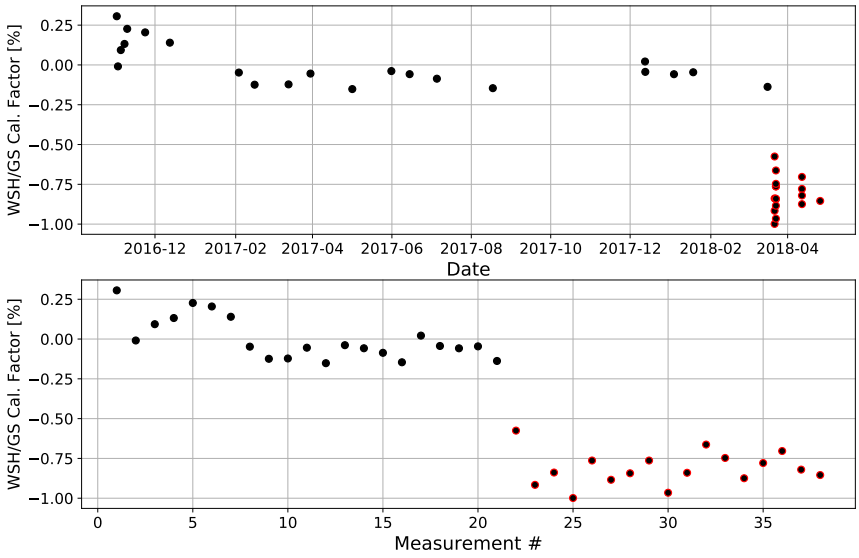


Figure 3: WSH/GS measurements from 2017-present (shown by date and index). Red-outlined points highlight offset values.

As an additional check, three WSL/WSH measurements were taken and compared to a WSL/WSH measurement taken previous to the occurrence of the offset (right plot of Figure 4). For WSL/WSH, the ratio on either side of the offset is shown to be within .047% of the ratio on either side for WSH/GS.

$$(\frac{\text{WSL}}{\text{WSH}})_a * (\frac{\text{WSH}}{\text{WSL}})_b = 1.006935 \qquad (\frac{\text{WSH}}{\text{GS}})_b * (\frac{\text{GS}}{\text{WSH}})_a = 1.007414 \tag{8}$$

In the above equations, the $b$ subscript denotes measurements taken before the offset started, and the $a$ subscript denotes those taken after. From these ratio values we determine that the source of error is WSH. The following two sections will cover experiments performed to determine the source of the error and measurements taken to create a new configuration for the Standards.

# 3 Cause of Calibration Factor Offset

In this section we investigate the source of the calibration factor offset. We were able to rule out the multimeter (Appendix A) and beam splitter (Appendix B) as potential error sources, bringing our focus to the power sensor. We then determined that spectralon degradation within the integrating sphere (Appendix C) and contamination of the photodiode (Appendix D) do not contribute significantly to the calibration factor. The source of the error was found to stem from the alignment of the two spacer apertures.

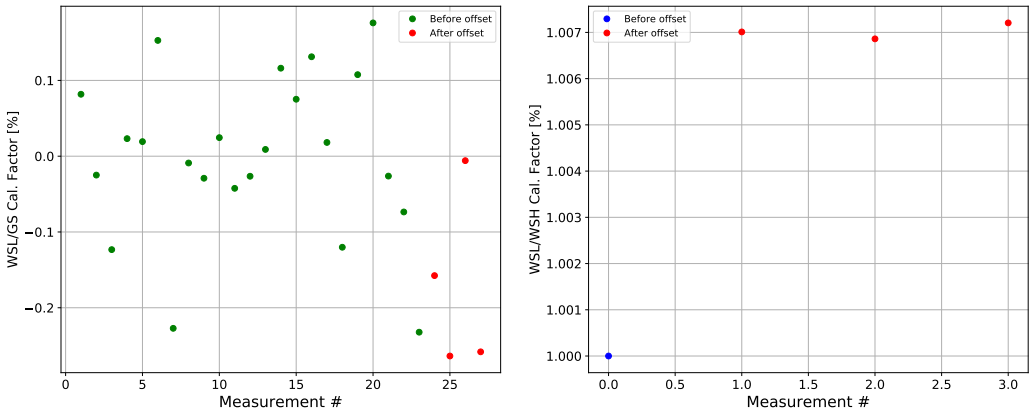


Figure 4: Left: WSL/GS measurements taken before (green) and after (red) the WSH/GS offset was seen. Right: WSL/WSH measurements taken before (blue) and after (red) offset was seen. Changes in WSL/WSH but not in WSL/GS indicate WSH as the error source.

### 3.1 Disassembly/Reassembly of Photodetector Spacers

As an additional check, the photodetector spacers and photodetector on WS1 were unscrewed and then reassembled onto the sphere. The concern was that the spacer apertures had become misaligned through reassemblies or mishandling of the instrument. A WS1/GS measurement was taken before the disassembly and reassembly procedure to ensure that it matched with previous measurements.

Afterwards WS1/GS measurements were taken, showing a 4% increase in calibration ratio values after the first reassembly. Following measurements after reassemblies resulted in a 6% drop and a subsequent 5% jump in ratio values (Figure 5). To understand the cause of these offsets, the power traveling through two slightly displaced spacers is examined.

Assuming the lower spacer is perfectly aligned with the integrating sphere aperture and the upper spacer with the photodiode aperture, the problem reduces to an equation of the area between two overlapping circular apertures:

$$A_{intersection} = 2R^2 cos^{-1}(\frac{x}{2R}) - x\sqrt{R^2 - \frac{x^2}{4}} \tag{9}$$

where R is the radius of each spacer aperture and x is the displacement from each other. The derivative of this with respect to displacement is:

$$\frac{\delta A}{\delta x} = -\sqrt{4R^2 - x^2} \tag{10}$$

The fractional change in power for a small displacement between spacers is determined by the fractional change in effective area of the overlapping apertures. Assuming the apertures begin perfectly aligned (x=0), the following equation is derived:

$$A_{intersection} \propto P \Rightarrow \frac{\delta P}{P} = \frac{\delta A}{A} = -\frac{2\delta x}{\pi R} \tag{11}$$

For a ∼1 mm aperture radius, a 0.1% shift in power corresponds to a spacer displacement of 1.57 $\mu$m. It seems very likely that this is the cause of the offset seen in WSH.

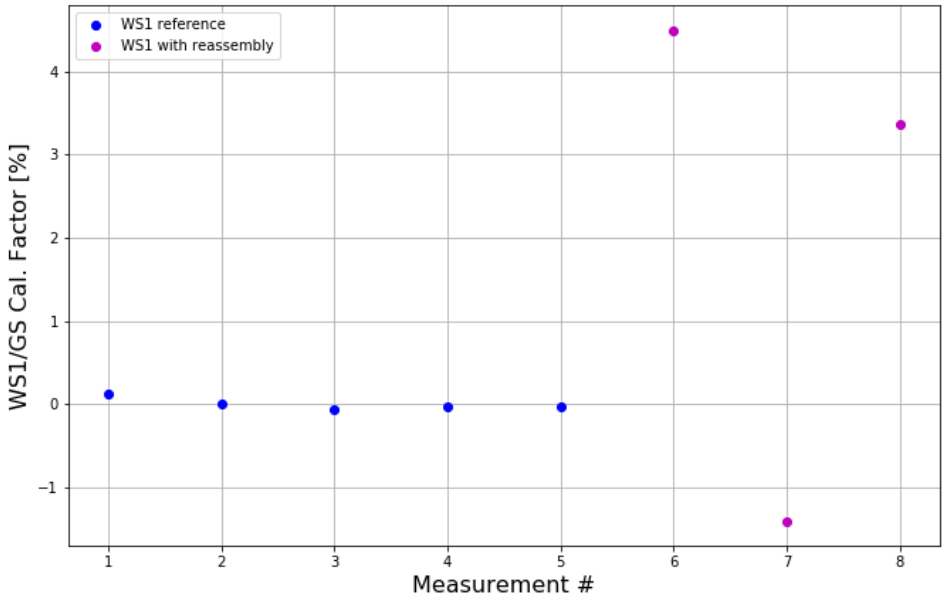


Figure 5: A sample of stable WS1/GS measurements made with no changes between measurements (blue), followed by measurements taken after disassembling/reassembling spacers (magenta).

# 4 Deciding on New Working Standard Configuration

This section describes the various experiments done to find an optimal configuration that minimize error on $\rho$.

## 4.1 Laser Speckle for Different Numbers of Spacers

A previous concern about the two-spacer system was that the surface area of the integrating sphere viewable to the photodiode would be small, creating a strong laser speckle effect on the calibration measurements. This was thought to be sufficiently alleviated by choosing a ten minute integration time with the intention of exceeding the coherence time for speckle. Calibration measurements were conducted with 0, 1, and 2 spacers attached to one integrating sphere and the other kept at 0 spacers as a control. The results of this are shown in Figure 14.

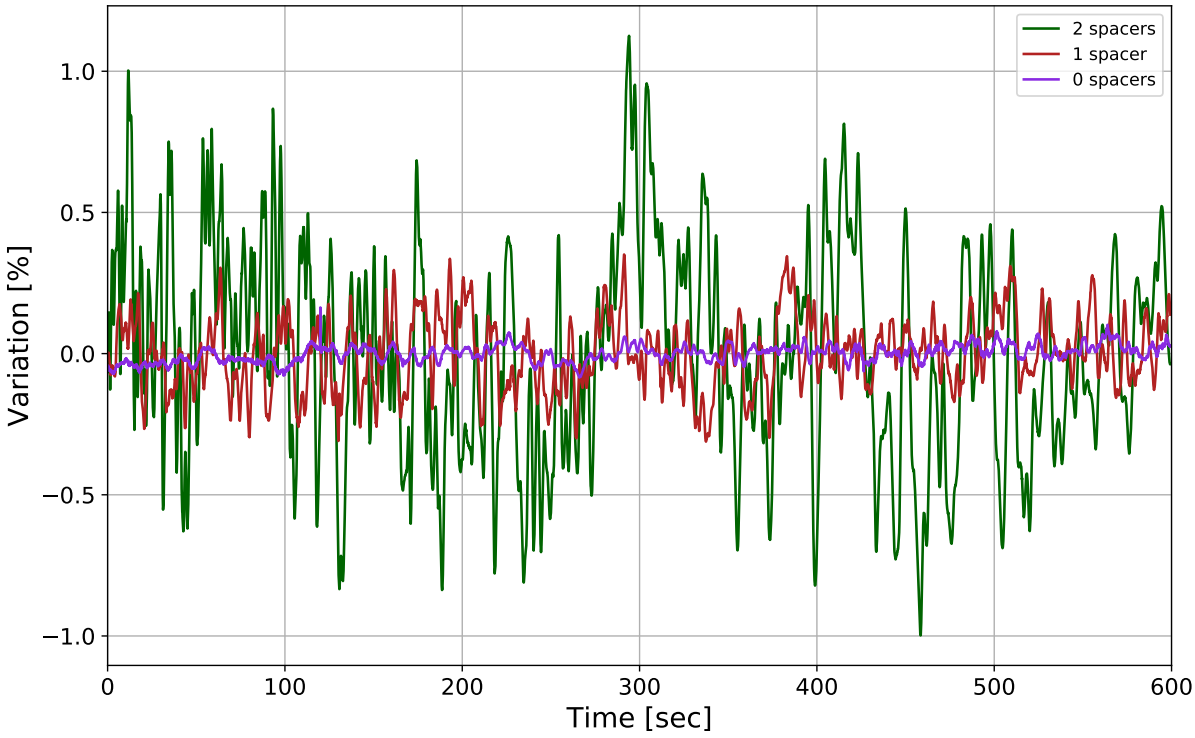


Figure 6: Power sensor output for three spacer configurations. Normalized time series are shown for two, one, and zero spacers. Zero spacers shows the lowest amount of laser speckle, and could reduce necessary integration time.

Both the one spacer and zero spacer systems have significantly lower laser speckle than the two spacer system. Switching to either of these configurations would reduce error due to speckle, as well as potentially reduce our required integration time.

### 4.2 Disassembly/Reassembly for Zero and One Spacers

We then test the sensitivity to disassembly/reassembly for one and zero spacer systems. In addition to testing the consistency the mounting mechanism, the standard deviation of disassembling/reassembling the three main setups can be treated analogously to the deviation that would be seen from bumps or strains that could occur during shipping of standards or as a result of mishandling. This also serves as a verification that the large variations measured when reassembling the two spacer setup were indeed dependent on the number of spacers.

Figure 7 shows zero and one spacer calibration factors after subsequent reassemblies. The spread of values is similar, with standard deviation listed below:

$$\text{Std. } (2) = 2.49897\% \qquad \text{Std. } (1) = 0.04503\% \qquad \text{Std. } (0) = 0.04023\% \tag{12}$$

Calibration factor values experience less variation for zero and one spacer setups by two orders of magnitude. The low level of variation also allows us to successfully make radial dependence measurements, which will be covered next.

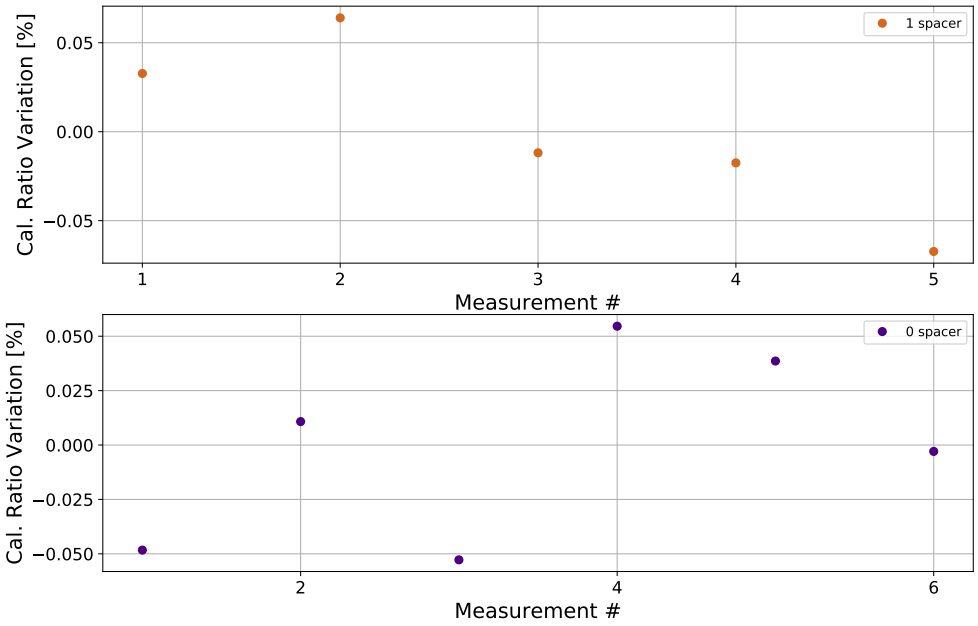


Figure 7: Calibration measurements taken after disassembling and then reassembling the photodetector mounting with zero spacers and one spacer. They both exhibit low levels of variation compared to the two spacer system.

### 4.3 Dependence on Radial Displacement of Photodetector/Spacers

The radial dependence of the photodetector connection is then tested by inserting washers of varying thicknesses between the joints in the zero and one spacer systems and measuring the power output relative to a reference sensor. The single joint in the zero spacer system and two joints in the one spacer system are individually displaced and plotted in Figure 8. Each plot has the variation in power measurement as a function of radial displacement at the joint.

After this measurement was taken, it was discovered that the slope of the port frame keeps it from sitting flush against the port adapter. This could potentially be a contributor to the zero and one spacer variation from Figure 7, and it also means that the thinner washers inserted between the joints in this experiment (∼0.1mm and under) are not reliable. The port adapters will be adjusted to fit to the ports.

The results show that the lowest and highest levels of radial dependence exist in the one spacer system. The lowest dependence is for radial variation in the spacer/sphere connection, and the highest is for the spacer/photodetector connection. While a single unit comprising

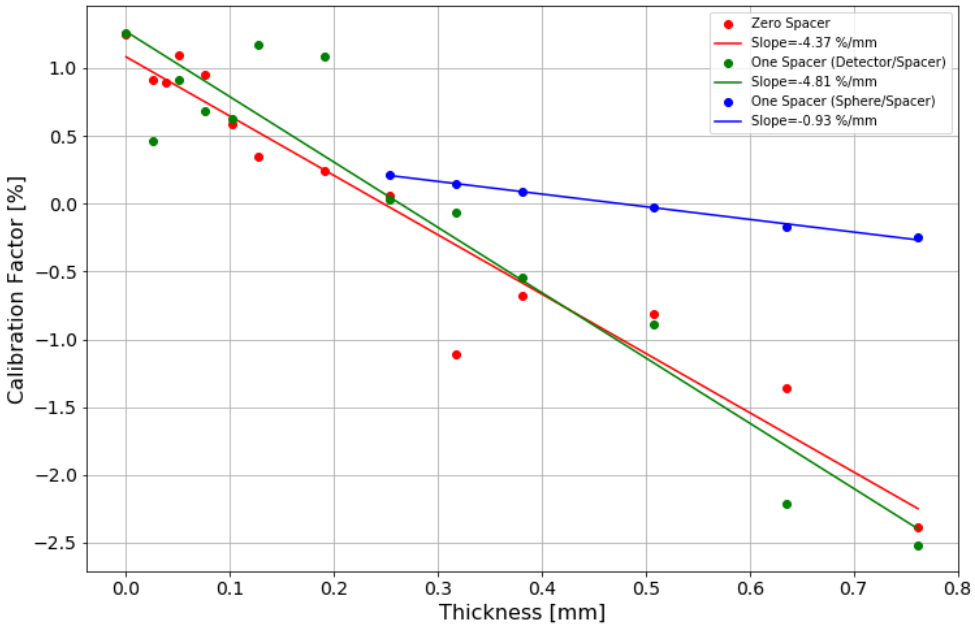


Figure 8: Radial dependence for the zero spacer and one spacer power sensor configurations. Radial dependence is tested by calculating the calibration factor with different thickness washers inserted in the joints between the photodetector and integrating sphere (this results in two separate measurements for the each joint in the one spacer configuration).

the spacer and photodetector would remove the highest term and present the least overall radial dependence by a factor of four, we have decided to prioritize low laser speckle and have a single unit, zero spacer photodetector housing designed. We believe this to be an acceptable route due to the low level of variability we have seen in the past, and in addition the photodetector housing will include a new port attachment system that should increase the mounting reliability.

### 4.4 Photodiode Current/Frequency Dependence

The removal of spacers from the Working Standard/Gold Standard setup greatly increases the current across the photodiode, which leads to worries about the linearity of the photodiode response. The current increases by a factor of 5.5 from a two spacer system to a one spacer system, and 23.6 from a one spacer system to a zero spacer system. The performance of the photodiode for different currents/frequencies is tested by sending a 1 W sinusoidal beam from the transmitter module and measuring the Total Harmonic Distortion (THD) of the photodiode output (Figure 9).

The THD of a signal is the ratio of power in its harmonics over the fundamental frequency. For a sinusoidal input signal, harmonics in the photodiode output are the result of nonlinear response. We attempt to characterize whether the THD and therefore the error in the response exceeds 0.1%. This is done for three aperture sizes in the photodetector adapter,

using around 0.5W and 1W beam inputs. NOTE: This measurement is partially dependent on the performance of the Optical Follower Servo (OFS).

Below 7000 Hz, the photodiode's response stays within 0.1% of its input signal, for a variety of input currents. This is deemed an acceptable signal response, and as added reassurance the smallest photodetector aperture (2mm) is chosen. We don't currently have an explanation for the trend deviation for the lowest input current, but it is believed to be an issue with part of our measurement configuration, as the 0.63 mA and 0.42 mA signals are both for the 2 mm aperture with different input powers.

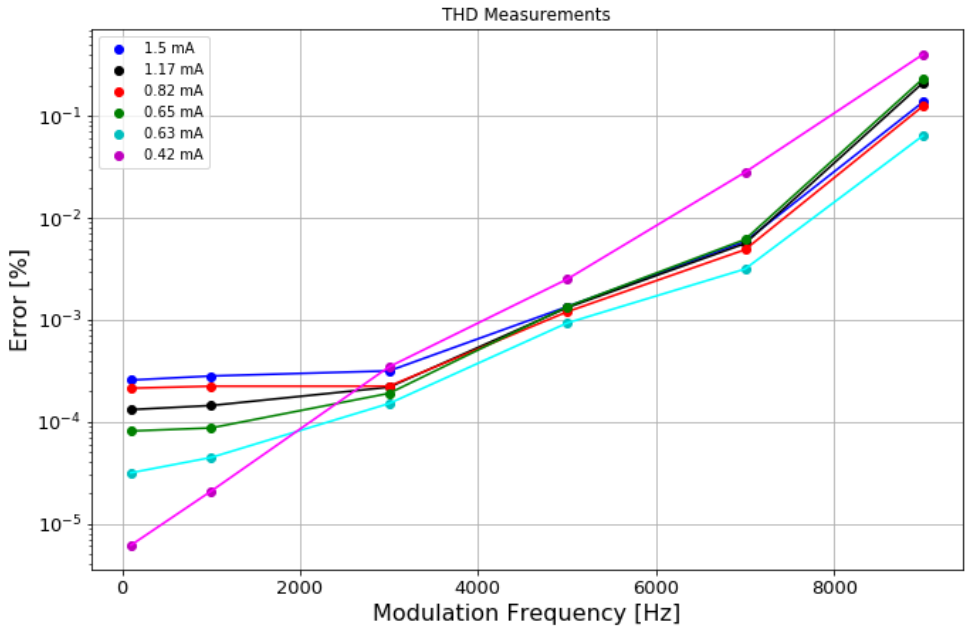


Figure 9: Error in photodiode response as a function of input beam frequency and current across the photodiode. The top two currents correspond to a 5 mm photodetector aperture, the next two to 3.5 mm, and the last two to 2 mm. Each aperture receives 1 W and 0.5 W input beams.

## 4.5 Implementing Circuitboard Transimpedance Amplifiers

In an effort to lower noise both in the system and the number of instruments we ship, a transimpedance amplifier was integrated into the circuitboard as a replacement for the external Keithley amplifier that was previously being used. This also allows for a transimpedance that is more specific to the power levels expected from the PCal laser (as opposed to the multiples of 10 provided by the Keithley).

For the new photodetector setup, there will be an expected 1-2 W of power entering the integrating sphere, as opposed to the current ∼100 mW laser power. We want to get a voltage measurement that is high above the noise level (up to the multimeter's ∼10 V limit) and keeps the current below ∼1.5 mA so that the power response remains roughly linear

(from the previous section). Knowing that we get approximately 1.16 V for $R_0$=3.5 mm aperture at $G_0 = 10^4$ V/A, and that we want to get around 10 V for $R_1$=2 mm aperture, we calculate the following:

$$I_1 = \frac{V_0}{G_0}(\frac{R_1}{R_0})^2 \qquad P_{rat} = \frac{P_1}{P_0}$$
$$I_1 \; P_{rat} \; G_1 = 10V$$
$$\Rightarrow G_1 = \frac{10V}{I_1 \; P_{rat}} = 2.8\text{e}4 \text{ V/A}$$

where I is the current, G is the gain, P is the power, and V is the voltage. To keep ourselves safely below the saturation point, we choose a gain factor of 2e4 V/A.

# 5 Final Configuration

In order to ensure consistent power sensor performance, the primary sources of error in the Working Standard configuration need to be mitigated. These main sources are recognized to be spacer occlusion, laser speckle, and radial dependence. We conclude that the best design setup for the photodetector has zero spacers, a single piece for the photodetector housing/adapter, improved photodetector mounting on the integrating sphere, and a circuit-board with a built-in transimpedance amplifier at 2e4 V/A.

# Appendix A: Checking Stability of Multimeter Voltage Response

In addition to checking the individual Working Standards, several tests were conducted to rule out other components of the calibration system as sources of the offset. The WSH, WSL, and GS Keithley 2100 multimeters were tested with a Martel voltage supplier to determine if they were properly calibrated. Given 1V, 1.5V, and 2V inputs, they all gave values accurate to within .05% (Table 1). The multimeters were thus determined not to be the source of the WSH/GS offset.

# Appendix B: Beam Splitter Temperature Dependence

The temperature dependence of the beam splitter is then tested. In the past, measurement by some researchers was conducted with the beam splitter obstructed by a beam dump before measurements began, whereas others would cover the individual integration spheres and let the beam splitter heat up while the laser stabilized. This could shift the reflection to transmission ratio as the laser increases the beam splitter temperature and change the mean of the time series.

| Multimeter Serial # | Input (V) | Output (V) |
|---|---|---|
| 758 | 1 | 1.00009 |
| | 1.5 | 1.5001 |
| | 2 | 2.0002 |
| 750 | 1 | 0.99999 |
| | 1.5 | 1.5000 |
| | 2 | 2.0000 |
| 559 | 1 | 0.99996 |
| | 1.5 | 1.5000 |
| | 2 | 1.9999 |

Table 1: Multimeter measurements with Martel voltage supplier inputs. The serial number is given as the identifying final three numbers.

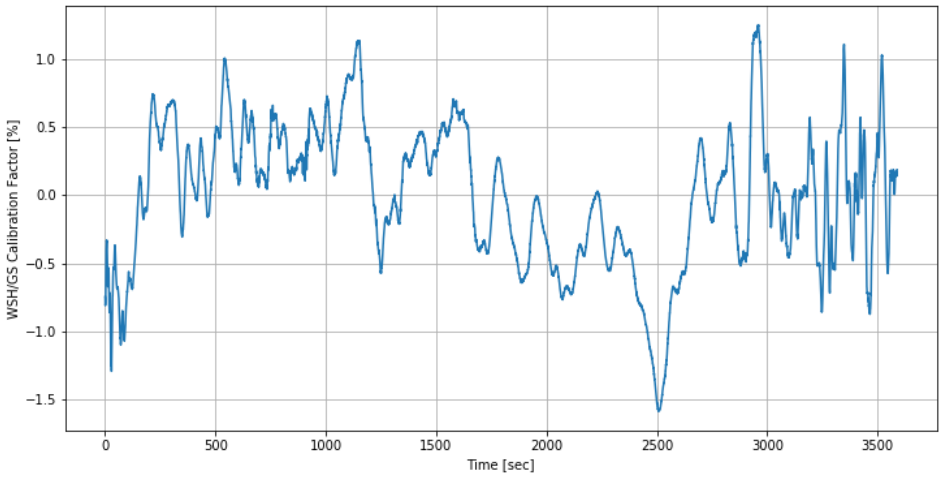


Figure 10: Plot of WSH/GS measurements as a function of index. Two measurements a second are taken for the duration of an hour.

To test this, an hour long WSH/GS integration was conducted where the beam splitter was covered until right before the measurement. The ratio between WSH and GS was then inspected to look for trends over time that could be correlated to a change in beam splitter index via temperature change. The results of this experiment are plotted in Figure 10.

The results show little variation that could be confidently attributed to a gradual increase in temperature. The existing variations have been attributed to laser speckle, which will be decreased by reducing the number of spacers between the integrating sphere and photodetector in the new GS design.

# Appendix C: Calibration Measurements While Varying Beam Input Angle

The recent addition of mounts was also given consideration, in case consistent centering of the laser beam in the integrating sphere could have degraded the sphere lining. This could alter the distribution of light in the sphere and cause a change in ratio values.

To test this, the mounts were removed and a set of WSH/GS ratio measurements was taken by roughly approximating the sphere locations and then aligning the beam to be in the center of the sphere aperture. The result of those measurements is shown in Figure 11. The left plot shows the measurements taken without a mount, the right is the set of twelve offset measurements taken previously with mounts (both normalized to their means).

The spread of values is comparable to the mounted measurement spread, and the mean values are close. From this we conclude that the position of the laser incidence on the integrating sphere is not the source of error.

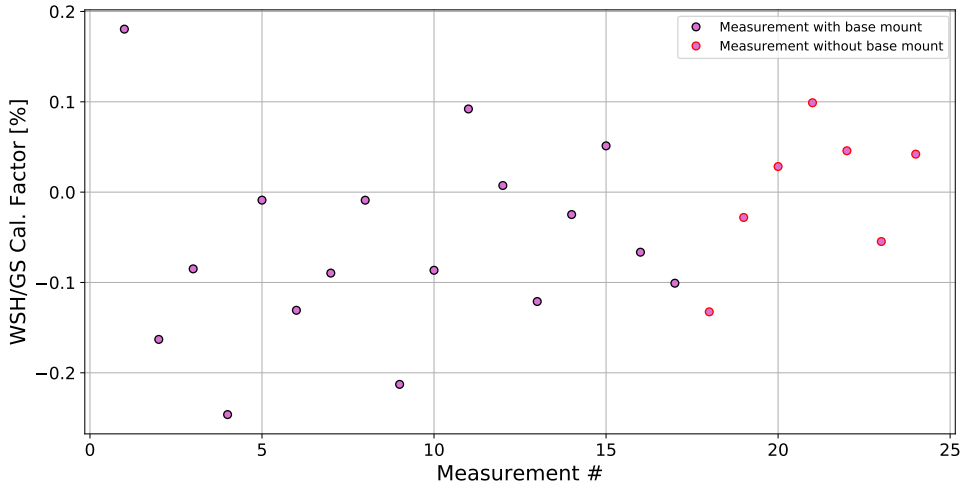


Figure 11: Plot of WSH/GS values taken with mounts removed and angles/distances varied relative to the beam splitter.

# Appendix D: Cleaning Photodiode with Isopropanol

Another theorized source of error was dust or condensation buildup in the photodetector. This issue had not been explored in detail previously for fear of altering the calibration values, but is now being tested on WS1, as it was already out of use.

First WS1 measurements were taken as a baseline measurement, as well as to determine the stability of the Working Standard after the fall. Four values were taken, yielding a 0.07% deviation. The power sensor was determined to have a low spread.

The photodetector was then detached from the spacer stack and taken apart. Some potential light smudging was observed and the photodiode glass was cleaned with isopropanol. Four more measurements were taken after this, displaying a 0.27% offset below the previous mean (Figure 12). While this offset is not insignificant, it does not go in the direction one would expect if a contaminant was removed from the photodiode. It is also less distinct than the 0.7% offset in WSH/GS. Thus condensation buildup is considered not to be the cause of the offset.

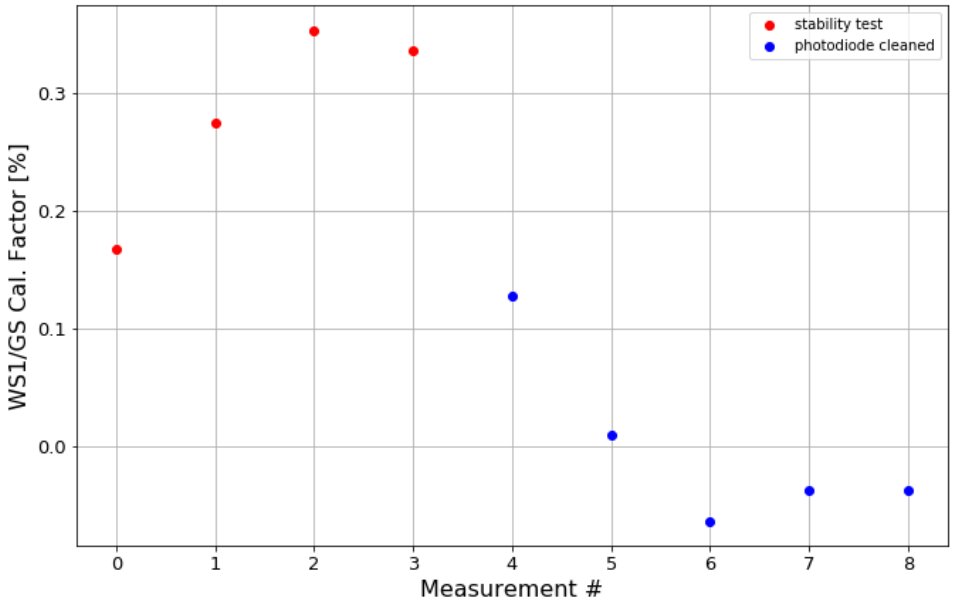


Figure 12: WS1/GS measurements taken before and after the photodetector plate was removed and the photodiode cleaned.